

Bright X-ray radiation from plasma bubbles in an evolving laser wakefield accelerator

M.S. Bloom,¹ M.J.V. Streeter,¹ S. Kneip,¹ R.A. Bendoyro,² O. Cheklov,³ J. M. Cole,¹ A. Döpp,^{1,4,5}
 C.J. Hooker,³ J. Holloway,⁶ J. Jiang,² N.C. Lopes,^{1,2} H. Nakamura,¹ P.A. Norreys,³ P.P. Rajeev,³
 D.R. Symes,³ J. Schreiber,^{1,4,5} J. C. Wood,¹ M. Wing,⁶ Z. Najmudin,¹ and S.P.D. Mangles¹

¹*The John Adams Institute for Accelerator Science, Imperial College London, London, SW7 2AZ, UK*

²*GoLP/Instituto de Plasmas e Fusão Nuclear, Instituto Superior Técnico, U.L., Lisboa 1049-001, Portugal*

³*Central Laser Facility, STFC Rutherford Appleton Laboratory, Didcot OX11 0QX, UK*

⁴*Fakultät für Physik, Ludwig-Maximilians-Universität München, D-85748 Garching, Germany*

⁵*Max-Planck-Institut für Quantenoptik, Hans-Kopfermann-Str. 1, D-85748 Garching, Germany*

⁶*Department of Physics and Astronomy, University College London, London WC1E 6BT, UK*

(Dated: January 15, 2023)

We show that the properties of the electron beam and bright X-rays produced by a laser wakefield accelerator can be predicted if the distance over which the laser self-focuses and compresses prior to self-injection is taken into account. A model based on oscillations of the beam inside a plasma bubble shows that performance is optimised when the plasma length is matched to the laser depletion length. With a 200 TW laser pulse this results in an X-ray beam with median photon energy of 20 keV, $> 10^9$ photons per shot and a peak brightness of 4×10^{23} photons $\text{s}^{-1}\text{mrad}^{-2}\text{mm}^{-2}(0.1\% \text{BW})^{-1}$.

Laser wakefield accelerators[1] have gathered increasing interest since it was first shown that they were capable of producing high quality electron beams[2–4]. Development has continued apace, and laser wakefield accelerators can now produce ultra-short bunches of electrons, down to a few femtoseconds[5], and reach multi-GeV beam energies[6–8]. One of the principal near-term applications of laser wakefield accelerators is the production of bright, femtosecond duration pulses of broadband X-rays[9, 10], that are suitable for a range of applications[11].

A laser wakefield accelerator is formed when an intense, short-duration laser pulse is fired into a moderate density plasma. The ponderomotive force associated with the laser pushes plasma electrons out of its way as it propagates. Due to the much heavier—effectively stationary—ions the electrons rush back towards their equilibrium position once the laser has passed, setting up a charge oscillation with a relativistic phase velocity in the wake of the laser pulse. When driven by a sufficiently intense laser pulse, almost all of the electrons can be expelled from an approximately spherical cavity behind the drive, known as the plasma bubble[12]. The electric fields inside this bubble can be capable of accelerating electrons to 1 GeV in just 1 cm[13].

Electrons can be self-injected into the bubble from the background plasma if the wave has a sufficiently high amplitude[14]. The three-dimensional structure of the bubble means that the injected electron beam undergoes betatron oscillations with a short wavelength ($\sim 100 \mu\text{m}$ for $\sim 1 \text{ GeV}$) and so generates synchrotron X-rays in the multi-keV spectral range[9].

In this letter we report on the experimental optimisation of the X-rays generated by a laser wakefield accelerator driven by a 200 TW laser. We show that the electron

and X-ray properties are well described by an analytical model that includes the fact that self-injection only occurs after the pulse has self-focused and self-compressed to a sufficiently high intensity. We also show that this source outperforms previous reports of X-ray emission from wakefield accelerators[7, 10].

The experiment was performed using the Astra Gemini laser at the Rutherford Appleton Laboratory, which delivered pulses of 12 J and duration 55 fs FWHM onto a supersonic gas jet target. The laser was focused with an $f/20$ off-axis parabolic mirror to a $22 \mu\text{m}$ FWHM spot containing $\approx 30\%$ of the energy. The peak intensity at focus in vacuum was $I \approx 2.2 \times 10^{19} \text{ Wcm}^{-2}$, corresponding to a normalised vector potential $a_0 = eA_0/(m_e c^2) \simeq 3$.

Two different helium gas jet targets with exit diameters of (10, 15) mm were used, producing approximately uniform density plasmas of length (8.5, 13) mm with electron densities up to $(8.0, 4.0) \times 10^{18} \text{ cm}^{-3}$ respectively. The laser was focused onto the front edge of the gas flow. The generated electron beam was analysed using a magnetic spectrometer consisting of a 30 cm long 1 T permanent dipole magnet and two scintillating (Kodak Lanex regular) screens.

The magnet also swept the electron beam away from an indirect detection X-ray CCD camera (Princeton Instruments PIXIS) placed on the laser axis. This was mounted outside the vacuum chamber behind a $180 \mu\text{m}$ thick Be window. An array of 16 metallic filters mounted on a thin Al/mylar substrate was placed directly in front of the camera's CsI scintillator.

The X-ray spectrum was found by performing a least squares fit to the signal detected behind each filter, taking into account the transmission through each filter and the absolutely calibrated detector response under the assumptions that the spectrum was spatially uniform over

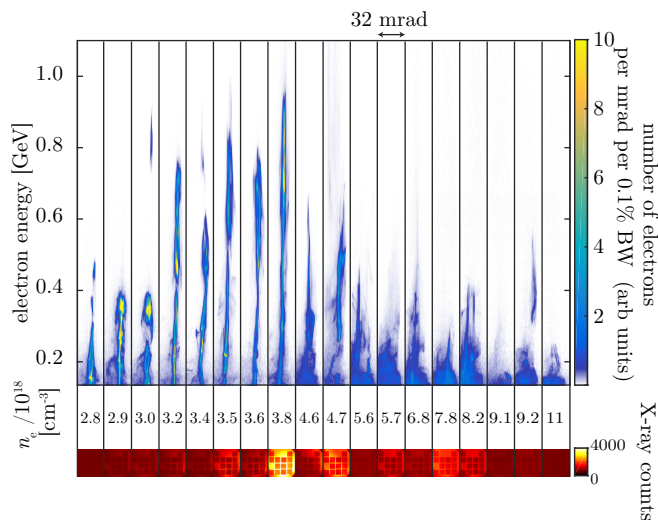


FIG. 1. Variation of electron and X-ray beams as a function of n_e for 10 mm nozzle. Top: Dispersion-corrected spectrally-dispersed images of the electron beam for a selection of shots. Bottom: X-ray CCD camera images for the same shots.

the detector and has a synchrotron-like shape given by: $d^2I/(dEd\Omega)_{\theta=0} \propto \xi^2 \mathcal{K}_{2/3}^2(\xi/2)$, where $\mathcal{K}_{2/3}(x)$ is a modified Bessel function of order $2/3$ and $\xi = E/E_c$. The shape of this spectrum is characterized by a single parameter, the critical energy, E_c [15]. Gaps between the X-ray filters and repeated filters allowed gradients in the X-ray beam profile to be taken into account.

Fig. 1 shows the variation of the electron beam spectrum and corresponding X-ray CCD images with plasma density for the 10 mm nozzle. Shots in this data sub-set correspond to the brightest X-ray image recorded at each density. The data shows that there is an optimum density for acceleration of $n_e \approx 3.8 \times 10^{18} \text{ cm}^{-3}$, and that the X-ray signal is correlated with the electron beam energy. Above the optimum density, the electron beam begins to develop transverse structure and increased divergence. This is consistent with the electron beam interacting with the plasma, driving its own wake and becoming susceptible to propagation instabilities[16]. As the electron beam dephases, it can also interact with the laser field[17] which can also increase the X-ray flux[18]. However, under these conditions no major enhancement in X-ray flux is evident due to these effects.

Fig. 2 shows the variation of the electron energy, W_{\max} with n_e for both the 10 and 15 mm gas nozzles. Both datasets show a similar trend; above a threshold density, W_{\max} rapidly increases until it reaches a maximum after which it decreases approximately $\propto \frac{1}{n_e}$. Both the threshold and optimum densities occur at lower densities for the 15 mm nozzle. As the X-ray signal is optimised when the electron beam energy is highest, optimisation of the

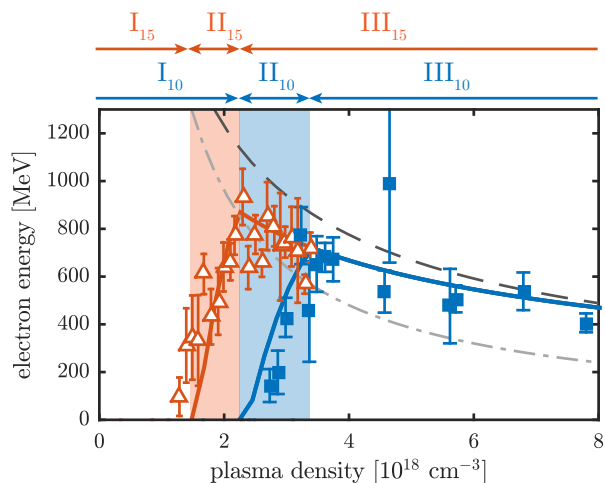


FIG. 2. Variation of W_{\max} with n_e for 10 (squares) and 15 mm (triangles) gas jets. Each point is the mean from $N = 1-5$ shots, bars represent the combined statistical and measurement errors. Curves show maximum energy predicted using: eqn. 1 (dot-dash); eqn. 3 (dash); eqn. 4 for the 10 mm (blue); and 15 mm (red) nozzles. The regions (I, II and III) described in the text are indicated for each nozzle. Region II for each nozzle is also indicated as a shaded region.

X-ray generation relies on understanding how to optimise the electron energy. The maximum energy predicted by Lu et al.,[19]:

$$W_{\max}/(m_e c^2) = \frac{2}{3} a_0 (n_c/n_e), \quad (1)$$

is plotted in fig. 2 (dot-dash line) using the a_0 for vacuum. Here $n_c = \epsilon_0 m_e \omega^2 / e^2$ is the critical plasma density for radiation with angular frequency ω . Eqn. 1 consistently underestimates the electron energy at high densities and does not predict an optimum density.

Eqn. 1 assumes a non-evolving laser pulse. However, self-focusing and pulse compression occur as the pulse propagates in its self-generated wakefield, causing a_0 to increase. The maximum value of a_0 can be calculated by assuming that the pulse evolves to a matched spot size that satisfies $a_0 \approx 2(P_f/P_c)^{1/3}$ [19], where $P_c = 2m_e c^3 n_c / (r_e n_e)$ is the critical power for relativistic self-focusing and r_e is the classical electron radius. The final power, P_f , depends on pulse compression and the amount of laser energy that is trapped in the bubble. For a fraction α of the total laser energy E_L compressed to a pulse duration τ_f , the resulting expression is:

$$a_{\max} \simeq 2(\alpha E_L / \tau_f P_c)^{1/3}. \quad (2)$$

Even though this expression does not include the effects of pump depletion and photon deceleration, it has been shown to be sufficiently accurate to predict the self-injection threshold[14]. The pulse compression can be

quantified by assuming that the front of the pulse travels at the linear group velocity in the plasma while the rear of the pulse, which sits in the significantly reduced plasma density inside the bubble, travels at c . For an initial pulse duration τ_0 , the pulse duration after propagation length l is then: $\tau_f(l) \approx \tau_0 - \frac{n_e l}{2c n_c}$ [20]. The maximum propagation length, L_{\max} , will be limited by pump depletion $L_{\text{pump}} \approx c\tau_0 n_c/n_e$ [19] or by the length of the target, L_{target} , if $L_{\text{target}} < L_{\text{pump}}$. So accounting for pulse evolution, the beam energy varies as:

$$W'_{\max}/(m_e c^2) \approx \frac{4}{3} (\alpha E_L / \tau_f P_c)^{\frac{1}{3}} (n_c/n_e) \quad (3)$$

Eqn. 3 is shown as the dashed line in fig. 2. This model overestimates the observed energy gain, only approaching the data at high densities. It also still fails to explain the initial increase in beam energy with increasing density. These features can be explained by including a distance over which the a_0 amplification occurs before self-injection. We call this the pre-injection pulse evolution length, L_{PIPE} . This PIPE length will decrease at higher densities as the pulse evolution rates increase [21]. The variation of electron energy with density can be split into three regions. At low density (region I), the PIPE length is longer than the gas jet and so no electrons are injected.

As the density is increased, the evolution becomes fast enough that injection occurs before the end of the gas jet, resulting in low energy electron beams. This region II is marked by the shaded area in fig. 2. Increasing the density further reduces the PIPE length and brings the injection point earlier in the gas jet. But in region II, the density is low enough that the laser has not depleted by the end of the gas jet, so earlier injection leads to an increase in acceleration length. This coupled with the increase in the accelerating field ($\propto \sqrt{n_e}$) results in a rapid increase of beam energy with increasing density.

Once the density is high enough that the pump depletion length is less than the gas jet length (region III), increasing the density actually decreases the length over which the electron beam is accelerated. Therefore in region III, despite the continuing increase in electric field strength, higher density results in a decrease in the electron energy. At the highest densities, the PIPE length is very short and, because the pump depletion length is longer than the dephasing length, the electron beam energy approaches the dephasing limit (eqn. 3).

To model this behaviour, we assume that the PIPE length $L_{\text{PIPE}} = S n_c/n_e$, where S is a constant of proportionality to be determined. The fraction of the dephasing length, $L_\phi = \frac{4}{3} a_0^{1/2} (n_c/n_e) c/\omega_p$, that the acceleration occurs over is therefore $\Delta_{\text{acc}} = (L_{\max} - L_{\text{PIPE}})/L_\phi$.

In the bubble regime, the electric field strength varies linearly inside the bubble, so that the beam energy varies quadratically according to:

$$W''_{\max} = W'_{\max} (2\Delta_{\text{acc}} - \Delta_{\text{acc}}^2). \quad (4)$$

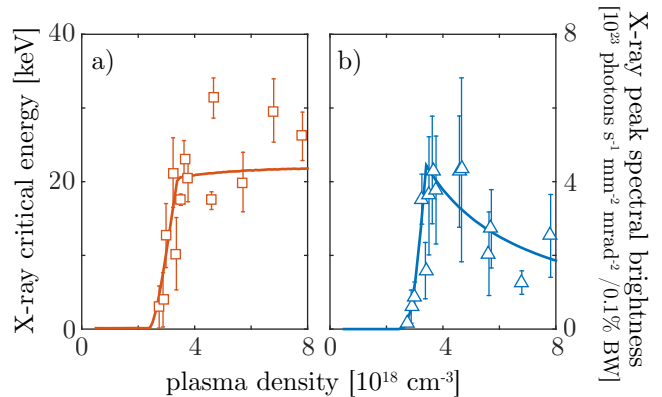


FIG. 3. Observed X-ray: a) E_c and b) \mathcal{B}_0 as a function of n_e for the 10 mm nozzle. Each point is the mean of $N = 1-5$ shots, bars represent the combined statistical and measurement errors. Curves show predictions using eqn. 6.

Eqn. 4 is plotted in fig. 2 (solid red and blue lines) with a single fitting parameter, $S = 11.9 \mu\text{m}$, chosen to best reproduce the experimental trend using a least squares fit. A detailed study of the laser pulse properties after the interaction show that the length over which power amplification due to pulse compression occurs is closely matched to this PIPE length [22]. The PIPE model reproduces all of the main features of the experimentally observed variation in electron energy including: the rapid rise to an optimum density; the reduction in optimum density for the longer nozzle; and the slower fall-off of maximum energy at higher densities. The model performs equally well for both the 10 and 15 mm nozzles with the same value for S , indicating that the precise shape of the gas density plays a minor role in determining the evolution as compared to the initial laser parameters. One of the main results of this model is that the density which maximises the electron beam energy for a fixed length target occurs when the length of the target equals the pump depletion length.

Fig. 3 plots how the X-ray critical energy, E_c , and peak brightness, \mathcal{B}_0 , vary with n_e for the 10 mm gas nozzle. Both the critical energy and brightness show similar behaviour; rapidly increasing as the density is increased before turning over above $n_e \approx 3.8 \times 10^{18} \text{ cm}^{-3}$. The critical energy reaches $E_c \approx 30 \text{ keV}$. The brightness, calculated assuming a constant duration matching that of the laser pulse (55 fs) and an r.m.s. source radius consistent with previous measurements ($1 \mu\text{m}$), reaches $4 \times 10^{23} \text{ photons s}^{-1} \text{ mrad}^{-2} \text{ mm}^{-2} (0.1\% \text{ BW})^{-1}$. This is significantly higher than previous results at lower laser power, e.g. [10], primarily due to the ability to accelerate electrons to $\sim \text{GeV}$ energies, thus increasing their ability to radiate. Under optimum conditions, a total photon yield of $N_X \approx 3 \times 10^9$ per shot was measured.

Calculations of the radiation emitted by self-injected electrons oscillating in the plasma bubble as they are accelerated and then decelerated from the back of the bubble to the front, i.e. over a distance $L = 2L_\phi$, have been presented in [23]. The number of betatron oscillations is found to be, $N_\beta = \gamma_p$, where γ_p is the Lorentz factor associated with the bubble motion. The resulting X-ray spectrum is synchrotron-like with an enhanced high-energy tail. To model the X-ray emission for an arbitrary acceleration length less than $2L_\phi$, the expressions from [23] can readily be modified. The modified spectrum for a beam of $N_b \approx 3.1 \times 10^8 \lambda_0 \sqrt{P_f}$ electrons[24] is:

$$\frac{d^2I}{d\omega d\Omega} = \gamma_p \frac{3e^2}{\pi^3 \epsilon_0 c} N_b \left(\frac{W'_{\max}}{m_e c^2} \right)^2 \mathcal{A} \left(\frac{\omega}{2\omega_{c0}}, \Delta_{\text{acc}} \right), \quad (5)$$

where $E_{c0} = \hbar\omega_{c0} = 7.75 \times 10^{-4} a_0^{5/2} (n_c/n_e)^{9/8}$ is the critical energy of a synchrotron spectrum corresponding to that emitted by an electron at the maximum energy W'_{\max} . The spectral shape function, $\mathcal{A}(\xi, \Delta_{\text{acc}})$ is:

$$\mathcal{A} = \xi^2 \int_{-1}^{\Delta_{\text{acc}}-1} (1-x^2)^{-\frac{3}{2}} \mathcal{K}_{2/3}^2 \left(\xi(1-x^2)^{-\frac{7}{4}} \right) dx. \quad (6)$$

The calculated variation in E_c and \mathcal{B}_0 have been overlaid on the experimental data in fig. 3a & b, respectively, for a plasma length of 8.5 mm with $L_{\text{PIPE}} = S n_c/n_e$ and $S = 11.9 \mu\text{m}$. The model, which has no fitting parameters other than than the PIPE length determined from the electron data, is consistent with the data. It exhibits the same the sharp initial rise and slow fall off for both E_c and \mathcal{B}_0 . The model shows that the X-ray emission is also optimised for $L_{\text{PIPE}} + L_{\text{acc}} \simeq L_{\text{target}}$.

Fig. 4 compares our measured E_c and \mathcal{B}_0 with previous experiments. Kneip et al. [24] calculated the following scaling laws in terms of the laser power, P (in TW) for both E_c (in keV) and \mathcal{B}_0 (in photons $\text{s}^{-1} \text{mrad}^{-2} \text{mm}^{-2} (0.1\% \text{BW})^{-1}$):

$$E_c = 3.4 \times 10^{-2} (\beta \alpha P)^{\frac{5}{6}} (n_c/n_e)^{\frac{7}{24}}, \quad (7)$$

$$\mathcal{B}_0 = 2.7 \times 10^{19} (\beta \alpha P)^{\frac{2}{3}} (n_c/n_e)^{\frac{19}{12}}, \quad (8)$$

where a power amplification factor, β is included to account for pulse compression. Compression over a depletion length at the rate in [20] gives $\beta = 2$.

Eqns. 7 and 8 treat P and n_e as independent parameters. However, increasing P decreases the threshold density for self-injection, n_{th} , so experiments at higher power typically operate at lower density[25]. Using [14] to find $n_{\text{th}}(P)$, we can therefore eliminate n_e from the above expressions. Furthermore experiments are typically optimised just above the threshold, so the curves for E_c and \mathcal{B}_0 (plotted in fig. 4) span the range $[n_{\text{th}}, 3n_{\text{th}}]$.

The scaling laws and experimental data both show that higher power lasers produce higher energy and brighter X-ray sources. However it is important to note that experiments can differ significantly from the scaling law.

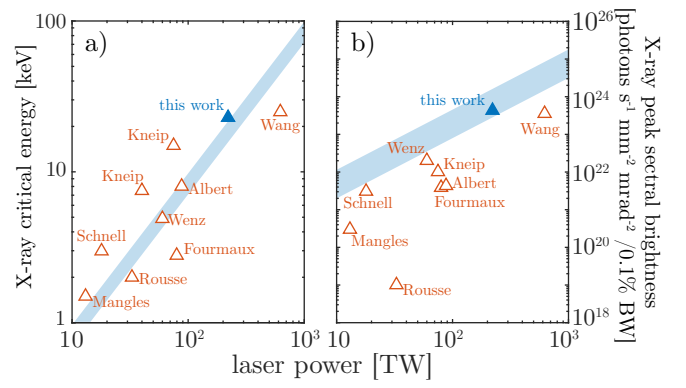


FIG. 4. Scaling of X-ray radiation with laser power from various experiments [9, 10, 26–30]: a) E_c ; b) \mathcal{B}_0 . The shaded region corresponds to eqns. 7 and 8 for $n_{\text{th}} \leq n_e \leq 3n_{\text{th}}$.

For example, higher photon energies can be produced if asymmetries are present in the wake which increase the betatron oscillation amplitude and so increase the source size and can decrease the brightness[26].

The photon source in our experiments is much brighter, and at higher photon energy than those at lower power[10] and comparable to an unoptimised experiment at five times higher laser power[7]. Our experimental data and the model developed here suggest that a significant increase in the flux of X-ray radiation from a laser wakefield accelerator can be achieved by careful optimisation of the length and plasma density for a given laser system, and so greatly broaden the range of applications that are accessible with these sources[11].

The authors thank the staff at the Central Laser Facility, Rutherford Appleton Laboratory for their assistance. This research was supported by STFC (ST/J002062/1, ST/P000835/1), EPSRC (EP/I014462/1), and the European Research Council (ERC) under the European Union's Horizon 2020 research and innovation programme (Grant Agreement No. 682399). The authors confirm that the all data used in this study are available without restriction. Data can be obtained by contacting plasma@imperial.ac.uk.

-
- [1] T. Tajima and J. M. Dawson, Physical Review Letters **43**, 267 (1979).
 - [2] S. P. D. Mangles, C. D. Murphy, Z. Najmudin, A. G. R. Thomas, *et al.*, Nature **431**, 535 (2004).
 - [3] C. G. R. Geddes, C. Toth, J. van Tilborg, E. Esarey, C. B. Schroeder, D. Bruhwiler, C. Nieter, J. Cary, and W. P. Leemans, Nature **431**, 538 (2004).
 - [4] J. Faure, Y. Glinec, A. Pukhov, S. Kiselev, S. Gordienko, E. Lefebvre, J. P. Rousseau, F. Burgy, and V. Malka, Nature **431**, 541 (2004).
 - [5] O. Lundh, J. Lim, C. Rechatin, L. Ammoura, A. Ben-

- Ismail, X. Davoine, G. Gallot, J.-P. Goddet, E. Lefebvre, V. Malka, and J. Faure, *Nature Physics* **7**, 219 (2011).
- [6] W. P. Leemans, A. J. Gonsalves, H. S. Mao, K. Nakamura, C. Benedetti, C. B. Schroeder, C. Tóth, J. Daniels, D. E. Mittelberger, S. S. Bulanov, J. L. Vay, C. G. R. Geddes, and E. Esarey, *Physical Review Letters* **113**, 245002 (2014).
- [7] X. Wang, R. Zgadzaj, N. Fazel, Z. Li, *et al.*, *Nature Communications* **4**, 1988 (2013).
- [8] H. T. Kim, K. H. Pae, H. J. Cha, I. J. Kim, T. J. Yu, J. H. Sung, S. K. Lee, T. M. Jeong, and J. Lee, *Physical Review Letters* **111**, 165002 (2013).
- [9] A. Rousse, K. T. Phuoc, R. C. Shah, A. Pukhov, E. Lefebvre, V. Malka, S. Kiselev, F. Burgy, J. P. Rousseau, D. P. Umstadter, and D. Hulin, *Physical Review Letters* **93**, 135005 (2004).
- [10] S. Kneip, C. McGuffey, J. L. Martins, Martins, *et al.*, *Nature Physics* (2010), 10.1038/nphys1789.
- [11] F. Albert, A. G. R. Thomas, S. P. D. Mangles, S. Banerjee, S. Corde, A. Flacco, M. Litos, D. Neely, J. Vieira, Z. Najmudin, R. Bingham, C. Joshi, and T. Katsouleas, *Plasma Physics and Controlled Fusion* **56**, 084015 (2014).
- [12] A. Pukhov and J. Meyer-ter Vehn, *Applied Physics B: Lasers and Optics* **74**, 355 (2002).
- [13] S. Kneip, S. R. Nagel, C. Bellei, N. Bourgeois, *et al.*, *Physical Review Letters* **100**, 105006 (2008).
- [14] S. P. D. Mangles, G. Genoud, M. S. Bloom, M. Burza, Z. Najmudin, A. Persson, K. Svensson, A. G. R. Thomas, and C. G. Wahlström, *Physical Review Special Topics - Accelerators and Beams* **15**, 011302 (2012).
- [15] This definition of E_c is different to that used in refs [13, 31] but consistent with refs [9, 32, 33]).
- [16] C. M. Huntington, A. G. R. Thomas, C. McGuffey, T. Matsuoka, V. Chvykov, G. Kalintchenko, S. Kneip, Z. Najmudin, C. Palmer, V. Yanovsky, A. Maksimchuk, R. P. Drake, T. Katsouleas, and K. Krushelnick, *Physical Review Letters* **106**, 105001 (2011).
- [17] S. P. D. Mangles, A. G. R. Thomas, M. C. Kaluza, O. Lundh, F. Lindau, A. Persson, F. S. Tsung, Z. Najmudin, W. B. Mori, C. G. Wahlström, and K. Krushelnick, *Physical Review Letters* **96**, 215001 (2006).
- [18] S. Cipiccia, M. R. Islam, B. Ersfeld, R. P. Shanks, *et al.*, *Nature Physics* **7**, 867 (2011).
- [19] W. Lu, M. Tzoufras, C. Joshi, F. S. Tsung, W. B. Mori, J. Vieira, R. Fonseca, and L. Silva, *Physical Review Special Topics - Accelerators and Beams* **10**, 061301 (2007).
- [20] J. Schreiber, C. Bellei, S. P. D. Mangles, C. Kamperidis, S. Kneip, S. R. Nagel, C. A. J. Palmer, P. P. Rajeev, M. J. V. Streeter, and Z. Najmudin, *Physical Review Letters* **105**, 235003 (2010).
- [21] W. Mori, *IEEE Journal of Quantum Electronics* **33**, 1942 (1997).
- [22] M. J. V. Streeter, S. Kneip, M. S. Bloom, R. A. Bendroyro, *et al.*, *ArXiv e-prints* (2017), arXiv:1710.05337 [physics.plasm-ph].
- [23] A. G. R. Thomas, *Physics of Plasmas* **17**, 056708 (2010).
- [24] S. Kneip, Z. Najmudin, and A. G. R. Thomas, *High Energy Density Physics* **8**, 133 (2012).
- [25] S. P. D. Mangles, *CERN Yellow Reports* **1**, 289 (2016).
- [26] S. P. D. Mangles, G. Genoud, S. Kneip, M. Burza, K. Cassou, B. Cros, N. P. Dover, C. Kamperidis, Z. Najmudin, A. Persson, J. Schreiber, F. Wojda, and C. G. Wahlström, *Applied Physics Letters* **95**, 181106 (2009).
- [27] M. Schnell, A. Sävert, B. Landgraf, M. Reuter, M. Nicolai, O. Jäckel, C. Peth, T. Thiele, O. Jansen, A. Pukhov, O. Willi, M. C. Kaluza, and C. Spielmann, *Physical Review Letters* **108**, 075001 (2012).
- [28] J. Wenz, S. Schleede, K. Khrennikov, M. Bech, P. Thibault, M. Heigoldt, F. Pfeiffer, and S. Karsch, *Nature Communications* **6**, 7568 (2015).
- [29] S. Fourmaux, S. Corde, K. Ta Phuoc, P. M. Leguay, S. Payeur, P. Lassonde, S. Gnedyuk, G. Lebrun, C. Fourment, V. Malka, S. Sebban, A. Rousse, and J. C. Kieffer, *New Journal of Physics* **13**, 033017 (2011).
- [30] F. Albert, B. B. Pollock, J. L. Shaw, K. A. Marsh, J. E. Ralph, Y. H. Chen, D. Alessi, A. Pak, C. E. Clayton, S. H. Glenzer, and C. Joshi, *Physical Review Letters* **111**, 235004 (2013).
- [31] E. Esarey, B. A. Shadwick, P. Catravas, and W. P. Leemans, *Physical Review E* **65**, 56505 (2002).
- [32] A. Rousse, K. T. Phuoc, R. C. Shah, R. Fitour, and F. Albert, *European Physical Journal D* **45**, 391 (2007).
- [33] J. D. Jackson, *Classical Electrodynamics*, 3rd ed. (Wiley, New York, 1999).